JACS JOURNAL OF THE AMERICAN CHEMICAL SOCIETY

Perspective

Cite This: J. Am. Chem. Soc. 2019, 141, 8382−8396

pubs.acs.org/JACS

Solid-State Ionics of Hybrid Halide Perovskites

Alessandro Senocrate* and Joachim Maier

Max-Planck-Institut fur Festkorperforschung, Heisenbergstraße 1, Stuttgart 70569, Germany

ABSTRACT: Many exciting "anomalies" affecting long-time and low-frequency phenomena in the photoactive halide perovskites that are presently in the focus of the field of photovoltaics turn out to be rather expected from the point of view of solid-state ionics. This Perspective discusses such issues based on the mixed conducting nature of these materials and indicates how the solid-state ionics toolbox can be used to condition and potentially improve these solids. In addition to equilibrium bulk properties, interfacial effects and light effects on the mixed conductivity are considered.

1. INTRODUCTION: THE SIGNIFICANCE OF ION CONDUCTION

Ion transport is crucial for various functions, mostly prominent for the field of energy research. Devices utilizing such functions include batteries, fuel cells, electrochemical sensors, and memristors. Of general relevance is the occurrence of mixed conductivity, where ionic and electronic conductivities are both appreciable. Mixed ionic−electronic conductors have been intensively studied in the field of solid-state ionics, with particular regard dedicated to the important material class of oxide perovskites. It will be shown here that many parallelisms exist with halide perovskites, which are presently heavily investigated for their potential use as efficient light-harvesters in photovoltaic devices.

Since the first observations of anomalous polarization phenomena in halide perovskite-based solar cells under operation,[1−7] and their clear attribution to ion transport,[8] a great deal of attention has been devoted to the investigation of the mixed conductivity in these materials.[9−29] The relevance of ion conduction for halide perovskites and devices is also due to its significance for degradation kinetics and for reaction processes shortening the lifetime of devices.[30−32] Moreover, ion transport is necessarily involved in the interaction of the materials with the surrounding atmosphere.[33] Last, but not least, ionic charge carriers are of great significance for space charge potentials building up at the interface with selective contact materials[34,35] (irrespective if these are generated under bias or already present in equilibrium) and are thus expected to affect carrier extraction and device performance.[36]

In this Perspective, we will focus on halide perovskite materials rather than devices and on reversible bulk ion (and electron) transport, which is inherently related to charge transport in devices. We will start out by describing the fundamentals of defect thermodynamics and kinetics, and by introducing solid-state ionics techniques commonly used to study mixed conductors. Here the mixed conducting oxide perovskite $SrTiO_3$ serves as a model material. This basis will help us understand the results presented later for halide perovskites, which in many ways behave similarly to their oxide counterparts. We will pay particular attention to the archetypal material MAPI (methylammonium lead iodide, $CH_3NH_3PbI_3$). We first describe the situation in the dark and then use the understanding gained there to extend the study to conditions under illumination. The peculiar light effects on ion transport observed in these materials will also be discussed.[37]

2. SOLID-STATE IONICS APPROACHES TO STUDY MIXED CONDUCTORS

In this section, first the general point defect thermodynamics underlying the compositional variation and transport properties of any ionic solid will be discussed. Second the defect kinetics will be addressed, which contains local changes in bulk defect concentrations as a function of time (i.e., transport and chemical diffusion theory) but also surface kinetics. In this context we also discuss techniques to separate ionic and electronic conductivities. To build the bridge between the well-understood oxide perovskites to the less-understood halide perovskites we will start out with oxide defect chemistry.

2.1. Defect Thermodynamics (Defect Chemical Modeling). It is a thermodynamic necessity that, at $T > 0$ K, any given material contains a certain quantity of point defects, due to the configurational entropy gain obtained upon deviation from the perfect crystal.[38−40] The concentrations of all these ionic and electronic point defects (hence including the relevant charge carriers) are functions of temperature, stoichiometry (δ), and dopant content.[39−41] Increasing temperature typically enhances defect concentrations and widens the stable stoichiometry range (Figure 1a). Notwithstanding the typically small variations in δ, the consequences for the defect concentrations are enormous, as these typically vary by orders of magnitude within such tiny window.[42] Consequently, while stoichiometry variations are usually negligible for properties such as volume, mass, or even phase energetics, they may massively influence functional features such as electrical, thermal, and optical properties.

Considering a model oxide MO, the oxygen partial pressure can be conveniently used as a parameter to vary stoichiometry. Qualitatively, the following can be stated: an increase in $P(O_2)$ enhances the concentrations of all the defects that increase the O-to-M ratio (i.e., δ), namely oxygen interstitials and metal vacancies. In addition, all defects decreasing the O-to-M ratio, such as oxygen vacancies and metal interstitials, will be suppressed. Increasing $P(O_2)$ also simultaneously enhances the electron hole concentration and decreases the conduction electron concentration. The effect of a dopant can also be

Received: December 20, 2018
Published: April 18, 2019

DOI: 10.1021/jacs.8b13594
J. Am. Chem. Soc. 2019, 141, 8382−8396

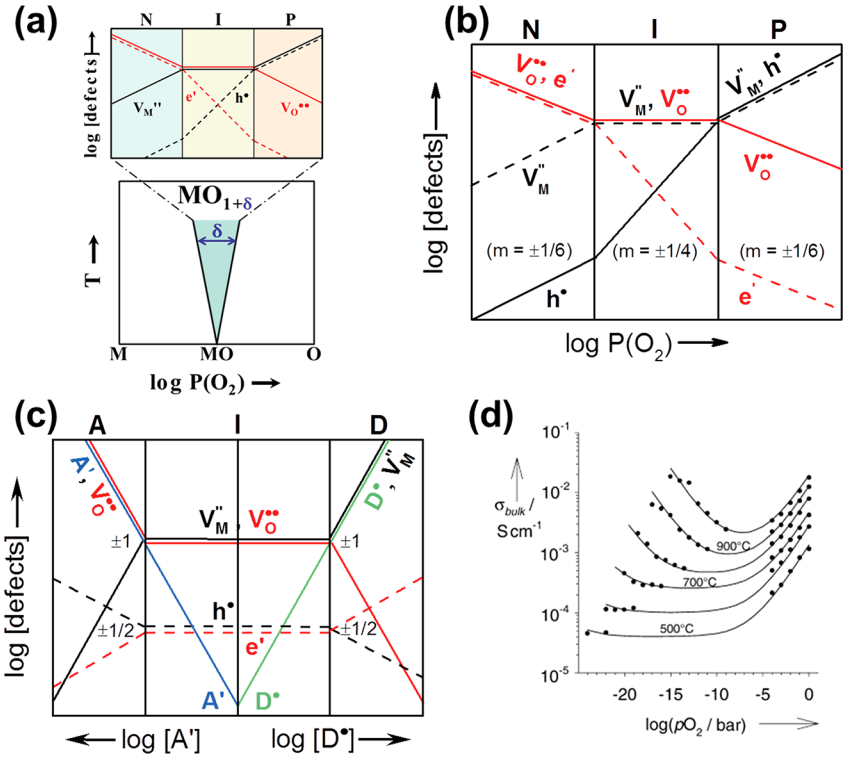

Figure 1. (a) Stability range of a binary oxide MO. The stable variations in stoichiometry the material can undergo (both in excess and in deficiency) are represented by the green window increasing with temperature. Within this window lies the entire defect diagram of the material, as given in detail in panel (b). (b, c) Double-logarithmic defect diagrams of a binary oxide MO, with Schottky-type intrinsic disorder as a function of (b) stoichiometry and (c) dopant content. Slopes are given on the figure. (d) Conductivity of slightly acceptor doped $SrTiO_3$ at different temperatures as a function of $P(O_2)$ showing p- and n-type electronic conduction at low and high $P(O_2)$, respectively, and predominant ionic transport in the intermediate region. Note that the experimental observation is entirely captured by the defect chemical modeling of panel (b). Panel (d) adapted with permission from ref 43. Copyright 2008 Wiley-VCH Verlag.

easily qualified. If the dopant is effectively negatively charged (interstitial foreign anions, substitutional cations of lower valence, substitutional anions of higher negative charge), the concentrations of negatively charged defects are depressed while the ones of positively charged defects are augmented. The opposite is true for effectively positively charged dopants (interstitial foreign cations, substitutional cations of higher valence, substitutional anions of lower negative charge). Doping necessarily affects all ionic and electronic defect concentrations, provided these are sufficiently mobile to be equilibrated.

To quantify the above considerations, the mass action laws for the defect reactions have to be addressed, together with the electroneutrality equation.[39−41] This assumes the establishment of a thermodynamic equilibrium between the point defects and the surrounding atmosphere and, in the simplest approach, considers dilute and randomly distributed point defects (defect interactions ignored). We consider again an oxide MO, for which we assume Schottky disorder (stoichiometric generation of metal ion and oxygen ion vacancies, V_M'' and $V_O^{••}$) to be the most relevant intrinsic defect reaction (point defects are here represented in the Kröger−Vink notation). The intrinsic ionic defect situation can thus be described by the following reaction and, for dilute conditions, by the related mass-action law:

$$M_M^x + O_O^x \rightleftharpoons V_M'' + V_O^{••} \qquad K_S = [V_M''][V_O^{••}] \tag{1}$$

M_M^x and O_O^x represent a metal ion occupying a regular metal site (oxide ion on oxygen site) with neutral effective charge. Considering the electronic side, the intrinsic electronic disorder reaction is the band-to-band transition:

$$\text{nil} \rightleftharpoons e' + h^• \qquad K_{el} = [e'][h^•] \tag{2}$$

Let us now consider a variation in the stoichiometry of MO upon changing the oxygen partial pressure. The corresponding reaction (and mass-action law) describing the effect on the defect concentrations is

$$\frac{1}{2}O_{2(g)} + V_O^{••} \rightleftharpoons O_O^x + 2h^• \qquad K_O = \frac{[h^•]^2}{[V_O^{••}]P(O_2)^{1/2}} \tag{3}$$

Combining eq 3 with the electroneutrality condition, we can predict the dependencies of the defect concentrations upon stoichiometry changes. The same approach can be used to quantify the effects of doping. The obtained defect concentrations are then usually plotted in double-logarithmic diagrams (known as Kröger−Vink diagrams), such as the ones given in Figure 1b,c for our model oxide MO.

In a ternary compound such as $SrTiO_3$, at not too high temperatures, the Sr/Ti ratio is fixed by the sample's history (synthetic conditions, previous high-temperature treatments), and as such cationic defects can be effectively considered as frozen dopants. As a consequence, defect diagrams similar to the MO case can be obtained, which have been directly experimentally observed (Figure 1d). More detailed considerations on this aspect are given in refs 44 and 45.

Analogous diagrams can then be obtained for MAPI (reported below in Figure 10), where changes in stoichiometry

DOI: 10.1021/jacs.8b13594
J. Am. Chem. Soc. 2019, 141, 8382−8396

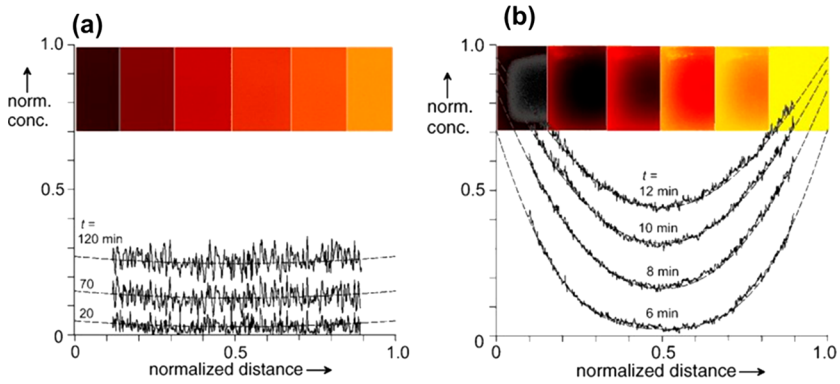

Figure 2. Limiting cases for oxygen incorporation in $SrTiO_3$: (a) surface-limited exchange and (b) diffusion-limited incorporation. Figure taken with permission from ref 43. Copyright 2008 Wiley-VCH Verlag.

are given by variations of the halogen partial pressure. The relevant defect equations (assuming frozen-in Pb defects) read as follows:

$$MA^{x}_{MA} + I^{x}_{I} \rightleftharpoons V'_{MA} + V^{\bullet}_{I} \qquad K_S = [V'_{MA}][V^{\bullet}_{I}] \tag{4}$$

$$\text{nil} \rightleftharpoons e' + h^{\bullet} \qquad K_{el} = [e'][h^{\bullet}] \tag{5}$$

$$\frac{1}{2}I_{2(g)} + V^{\bullet}_{I} \rightleftharpoons I^{x}_{I} + h^{\bullet} \qquad K_I = \frac{[h^{\bullet}]}{[V^{\bullet}_{I}]P(I_2)^{1/2}} \tag{6}$$

Note that MA^{x}_{MA} and I^{x}_{I} describe the occupancy of regular site by MA and I ions, respectively. This approach has also been successfully used to model the effects of doping[46] and of oxygen exposure[33] in MAPI. Note that in MAPI oxygen is an extrinsic—but still exchangeable—component. It is important to stress that, due to low temperatures normally used for MAPI, a relevant role may also be played by impurities or frozen-in native defects as compensating majority defects (this is also the case for $SrTiO_3$ at low temperatures). These aspects (even replacing Schottky by anti-Frenkel disorder), do not affect the general picture. The direct correspondence with experiments attests that defect chemical modeling is a very powerful tool for the identification of the dominant charge carriers.[33,46] We will discuss these aspects further below.

2.2. Defect Kinetics. While the thermodynamics is of great importance in determining how a material behaves upon changes in composition, in reality kinetic aspects play a decisive role. Most important is the kinetics of stoichiometry change (chemical process), which dictates the compositional changes effectively taking place and thus governs a material's kinetic stability as well. In order to connect with the detailed experience in the field of oxides, let us consider again $SrTiO_3$, equilibrated at a certain oxygen partial pressure. An increase (or decrease) in the outer $P(O_2)$ will provide the driving force for an oxygen flux directed inside (outside) the material. Though highly complex, the process can be viewed as a series of a surface step and a diffusion process. If the surface step is rate-limiting, the flux will—at least in proximity to equilibrium—depend on the inverse of a chemical resistance (Λ) and on the variation of the oxygen chemical potential (μ_0) at the surface:

$$j_O = -\Lambda_O \delta\mu_O = \bar{k}^{\delta}_{O}\delta c_O \tag{7}$$

Referring to δc_O as a driving force, $\bar{k}^{\delta}_{O}$ is an effective surface rate constant, which depends on the underlying mechanism of the surface reaction. The terms $\delta\mu_O$ and δc_O refer to the first bulk layer counted from the gas–solid interface, and they represent the difference between actual and final values (at $t = \infty$). In this limiting case, the stoichiometry will be homogeneous within the sample, as shown in Figure 2a, and the amount of oxygen incorporated will be a function only of surface rate constant and time. Atomistically, a surface incorporation reaction is composed of several steps, which include, for O_2, at least adsorption, electron transfer, O–O bond dissociation, and incorporation of atomic oxygen ions into the material. With the knowledge of the chemical reactions involved in the various steps, it is possible to relate them to experimentally accessible quantities such as the surface rate constant or the exchange rate. For more details the reader is referred to refs 41, 43, and 47. The other limiting case of interest is the one where the surface exchange rate is fast with respect to the bulk diffusion. In this situation, we can assume that the outer oxygen chemical potential will be established rapidly in the surface layer. As shown in Figure 2b, the concentration profiles obtained differ significantly from the previous case.

Due to the constraints set by the electroneutrality condition, this bulk diffusion of oxygen (and, in general, the diffusion of any component inside/outside a material) necessarily corresponds to the concentration change of a neutral component. The process is named chemical diffusion and occurs via coupled ionic and electronic transport processes. Considering the situation in which oxygen is mobile in MO, the transport from x to x′ can be described as follows:

$$\begin{array}{lll} O^{2-}(x) \rightleftharpoons O^{2-}(x') & & \text{ionic transport} \\ + \qquad + & & \\ 2e^{-}(x) \rightleftharpoons 2e^{-}(x') & & \text{electronic transport} \\ \updownarrow \qquad \updownarrow & & \\ O(x) \rightleftharpoons O(x') & & \text{chemical diffusion} \end{array} \tag{8}$$

These neutral compositional variations are governed by a chemical diffusion coefficient and thus by a chemical capacitance (C^{δ}) and by a chemical resistance (R^{δ}). The latter can be given as

$$R^{\delta} = R_{ion} + R_{eon} \tag{9}$$

and can be understood in terms of an effective mass transport for which both ionic and electronic diffusions are necessary. Similarly, the chemical capacitance can be described (for ionic and electronic defects of single charge) as

DOI: 10.1021/jacs.8b13594
J. Am. Chem. Soc. 2019, 141, 8382–8396

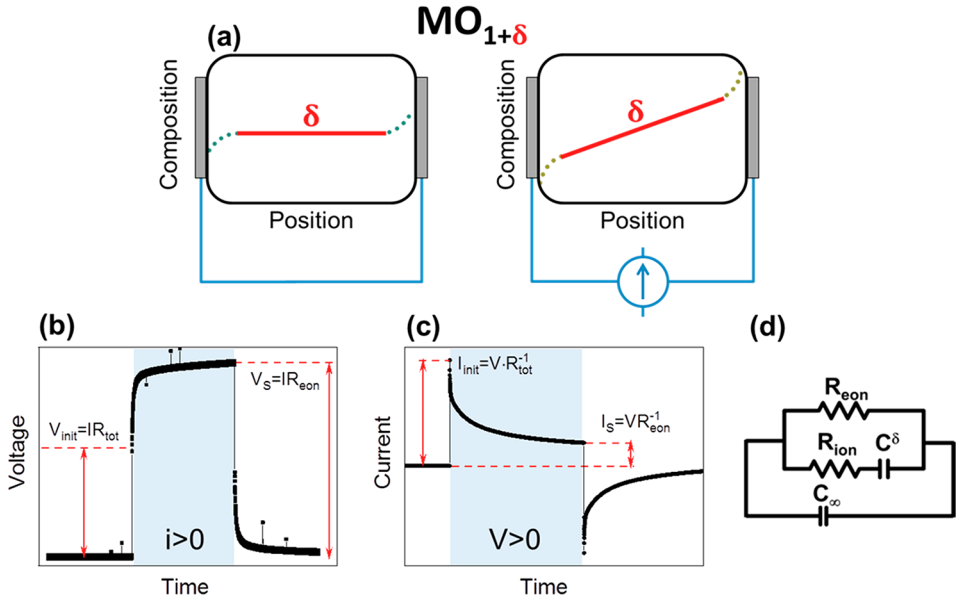

Figure 3. (a) Composition of a non-stoichiometric MO sample as a function of position with respect to ion-blocking partially reversible electrodes, with (right) or without (left) a d.c. current (or voltage). Note that, for perovskite structures, δ is typically negative. The corresponding bulk stoichiometric polarization affects the composition in the entire bulk. Space charge effects at the boundaries are indicated with dashed lines. (b) Galvanostatic and (c) potentiostatic polarization measurements, obtained by applying a constant current and a constant voltage, respectively. (d) Simplified equivalent circuit describing the chemical diffusion under galvanostatic conditions. For more precise evaluations, the circuit discussed in ref 53 has to be used.

$$C^{\delta} \propto \left(\frac{1}{c_{\mathrm{ion}}} + \frac{1}{c_{\mathrm{eon}}}\right)^{-1} \tag{10}$$

with c_{ion} and c_{eon} being the respective charge carrier concentrations. Equations 9 and 10 can be generalized to the presence of multiple carriers and internal reactions (trapping), as discussed in detail in refs 48 and 49. In general, C^{δ} represents the ability of a material to change its stoichiometry. These very important parameters also determine the characteristic time scale (τ^{δ}) of the chemical diffusion process, which can be given as

$$\tau^{\delta} = R^{\delta}C^{\delta} = \frac{4L^2}{D^{\delta}\pi^2} \tag{11}$$

Note that τ^{δ} is proportional to the square of the sample thickness (L). This is characteristic for such a diffusion process and comes from R^{δ} and C^{δ} both being proportional to L. Another characteristic feature of the diffusion process is that the time dependence follows a $\sqrt{t}$ law for short times and an exponential law for long times. The chemical diffusion coefficient can be generally expressed as

$$D^{\delta} = t_{\mathrm{ion}}D_{\mathrm{ion}}\chi_{\mathrm{ion}} + t_{\mathrm{eon}}D_{\mathrm{eon}}\chi_{\mathrm{eon}} \tag{12}$$

Note that D_{ion} and D_{eon} are defect diffusivities and are proportional to the mobilities of the dominant defects, while t_{ion} and t_{eon} are the ionic and electronic transport numbers (e.g., $t_{\mathrm{ion}} = \sigma_{\mathrm{ion}}/\sigma_{\mathrm{tot}}$). χ represents the differential trapping factors that are unity in the absence of internal defect interactions, as assumed in eq 10. Such kinetics of stoichiometry change takes place in every mixed conductor upon the application of an electrical or chemical potential difference and underlies fundamental processes such as mass storage. Importantly, the bulk diffusion does not only describe incorporation/excorporation of exchangeable components, but also internal compositional changes that can be generated by applying current or voltage across a mixed conducting material. We will pay particular attention to this latter case from now on, as it can be directly connected to experimental methods used to characterize mixed ionic-electronic transport.

When an electrical potential difference is applied across a sample sandwiched between two electrodes that are reversible for the electrons but not for the ions, a chemical diffusion process (as the one described above) will take place, with the potential difference as the driving force. The consequence is the progressive formation of a compositional gradient involving the entire bulk of the material.[50−52] In the steady state, $\nabla\mu_{\mathrm{ion}} \propto \nabla\phi$, and to a first approximation a linear δ profile occurs. Note that this is a bulk effect that does not generate excess charge locally. As schematized in Figure 3a, the stoichiometry of the material is, in these conditions, a function of the position between the electrodes. The case of symmetric boundary conditions (both electrodes reversible only for one of the carriers) has been described by Yokota,[52] while the case where on one side the electrode is reversible for both carriers by Wagner and Hebb.[50,51] This phenomenon (known as stoichiometric polarization) happens alongside space charge polarization, but on a completely different length (and time) scale. We will briefly mention this issue in the next section, but the interested reader is referred to the literature for more information.[34,35]

A stoichiometric polarization can be induced by applying a d.c. current or voltage, and we thus refer to a galvanostatic or potentiostatic measurement, respectively.[41] The typical electrical responses of a mixed conductor in these two experiments are reported in Figure 3b,c. Initially, both ionic and electronic charge carriers respond simultaneously to the electrical potential difference, yielding the sharp increase denoted as V_{init} or I_{init}. Subsequently, the blocking of the ionic species by the electrodes is progressively perceived, and via coupling with

DOI: 10.1021/jacs.8b13594
J. Am. Chem. Soc. 2019, 141, 8382−8396

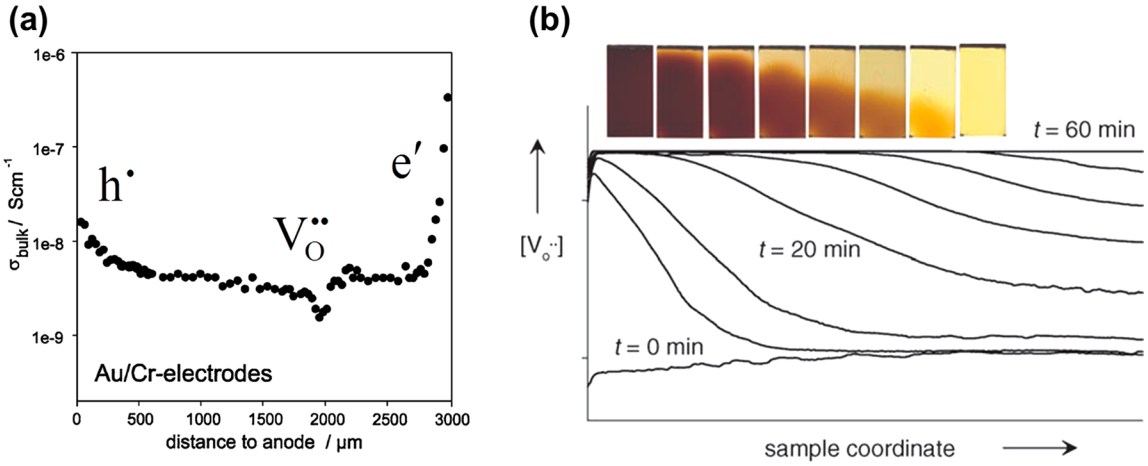

Figure 4. (a) Conductivity profile measured perpendicularly by microelectrodes after applying 300 V across a Fe-doped $SrTiO_3$ single crystal (electrodes placed at 0 and 3000 μm) for 90 min at 493 K. The analysis shows that the regimes of n-, vacancy-, and p-type conductivity are traversed. Panel (a) adapted with permission from ref 58. Copyright 2002 Kluwer Academic Publishers. (b) Oxygen vacancy concentration profiles in Fe-doped $SrTiO_3$ after abruptly changing $P(O_2)$ from 1 bar to 10^{-30} bar at 800 K. Snapshot of the quenched samples as a function of time, showing the moving of a diffusion front (oxygen loss takes place from the top). Panel (b) taken with permission from ref 43. Copyright 2008 Wiley-VCH Verlag.

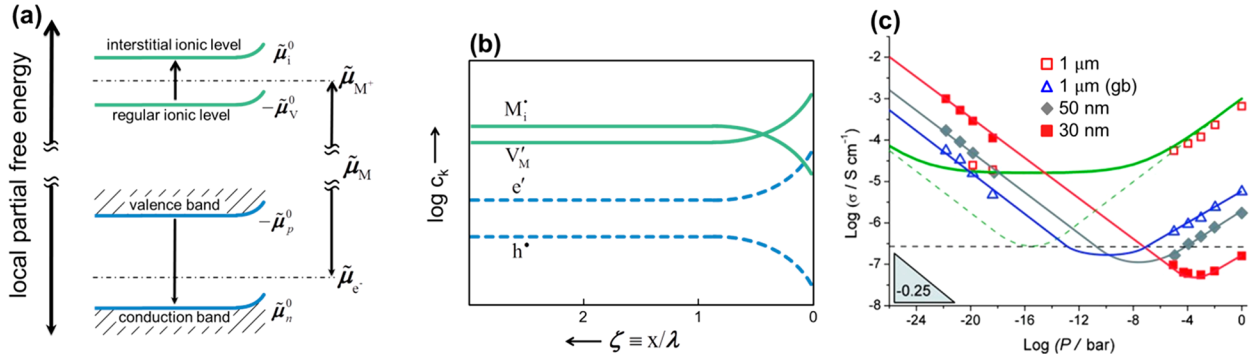

Figure 5. (a) Energy level diagram for ionic and electronic carriers at an interface in the case of predominant Frenkel disorder. Panel (a) taken with permission from ref 41. Copyright 2004 Wiley-VCH Verlag. (b) Defect concentration changes as a function of distance from a positively charged interface. All positive defects are suppressed, and all negative defects are enhanced close to the boundary. Panel (b) adapted with permission from ref 62. Copyright 1995 Elsevier Science Ltd. (c) Strong size effects on the conductivity of $SrTiO_3$ when entering the mesoscopic regime. Grain sizes of polycrystalline samples are given in the figure. Panel (c) adapted with permission from ref 63. Copyright 2010 Wiley-VCH Verlag.

electronic species a stoichiometric gradient forms. This steady-state situation, in which only the electronic carriers flow is represented by the reaching of a saturation current or voltage (V_S or I_S, see Figure 3b,c). Alternatively, the potential difference can be applied in a.c., and here we refer to high frequencies (bulk dielectric relaxation) or low frequencies (chemical diffusion). We will not discuss these measurement here, but more information on the impedance of mixed conductor can be found elsewhere.[53−55] Moreover, this situation also takes place when the electrical stimuli are triangular, as used in $i-V$ experiments. As there is no resting phase at the turning point of an $i-V$ curve, the stoichiometric polarization appears in the form of a hysteresis.[56] The comparison of the steady-state situation with the short time behavior (or with the high frequency response in impedance) allows one to separate the ionic and electronic resistances. This follows from the application of an equivalent circuit representing the mixed conductivity, which for galvanostatic conditions can be simplified to yield the circuit of Figure 3d. The generalized equivalent circuit that includes chemical effects can be found in the literature.[53] More information on the underlying chemical diffusion process can be extracted from the characteristic time scale of the polarization, which was previously described in eq 11. As already mentioned, the occurrence of the "square-root regime" is a typical signature of a chemical diffusion process. Nevertheless, in addition to these measurements it is well advised to use complementary evidence from electromotive force (emf) experiments, Faradaic reaction cells, permeation cells, chemical pumps, or similar to conclude on the presence of mixed ionic electronic transport.[41]

Significant complications may occur due to the presence of internal defect reactions (e.g., defect association/trapping), but also by strong deviation from equilibrium. For the former case, we refer the reader to the literature for a complete treatment of the problem and of its consequences on the electrical measurements described above.[49,57] The latter situation is realized in the case of high applied voltages/currents during a polarization experiment, but also for abrupt variations of stoichiometry. In these cases, the chemical diffusion coefficient ceases to be independent of the potential gradient (electrical or chemical). This leads to sharp concentration variations such as the ones shown in Figure 4a,[58] and even to the appearance of a proper diffusion front (Figure 4b).[59]

DOI: 10.1021/jacs.8b13594
J. Am. Chem. Soc. 2019, 141, 8382−8396

2.3. Defect Thermodynamics and Kinetics Involving Interfaces. The thermodynamic and kinetic situations described so far only apply to the bulk of the material under consideration. A further relevant field of study deals with ionic/electronic phenomena taking place at interfaces such as solid−solid (grain boundary, heterogeneous contacts) and solid−gas (material surface) interfaces. At the distance of the screening length (or below), distinct deviations from electroneutrality occur, and field effects determine the carrier concentrations. Figure 5a,b shows the correspondence of such field effects with concentration variations of electronic and ionic carriers. In fact in many materials, such as $SrTiO_3$, it is the ionic point defects which determine the field, while the electrons follow such field undergoing a "fellow traveler" effect. These phenomena are described in detail in ref 36. The deliberate introduction of interfaces (or more generally charged higher-dimensional defects) can be used as a materials design strategy in a similar way as the classic (zero-dimensional) doping. We speak then of heterogeneous (or higher-dimensional) doping. Such effects can lead to large variations in ionic and electronic charge carrier concentrations and can thus determine the macroscopic functional properties of a material given a high enough density of heterogeneities (e.g., in mesoscopic structures, see Figure 5c). The promising field that investigates these systems is called nano-ionics, and its general relevance for electronics and information technology is discussed elsewhere.[60] Interfaces of interest in our context are homophase boundaries (grain boundaries) but also heterophase boundaries such as oxide/halide interfaces.[36,61]

The intrinsic situation is more complex if deviations from equilibrium are allowed. Then kinetic space charges can build up even in the absence of equilibrium charges. The most important issue here is space charge polarization, which complements the stoichiometric polarization discussed before. In contrast to the latter, the relaxation time of space charge polarization is typically much shorter and can be given as

$$\tau_{sc} \approx R_{ion} C_{sc} \propto \frac{\varepsilon L}{\sigma_{ion} \lambda} \tag{13}$$

where ε is the dielectric constant and λ is the screening length. It is worthy of mention that, in the literature dealing with halide perovskites, the effect of ion conduction is typically ascribed to space charge polarization, instead of the above-described bulk polarization, disregarding the different time constants (cf. eqs 11 and 13).

2.4. Defect Thermodynamics and Kinetics under Light. So far, we have not considered light effects. Under illumination with light of energy above bandgap, the continuity condition has to be complemented by generation/annihilation terms for the electronic carriers. Here we are considering the steady-state situation under uniform and constant illumination, where the large photogeneration of electrons and holes, after deducting rapid recombination processes, yields an effectively increased concentration of electronic carriers. The defect chemical considerations given previously approximately apply to the steady state, but only if the radiation effects are sufficiently quick. Interesting light effects on the ionic defect concentrations could be imagined in the case where electrons and holes are kinetically decoupled. We will show below that indeed light effects on ionic transport are not only perceptible, but very substantial in MAPI.

3. ION CONDUCTION IN HYBRID HALIDE PEROVSKITES

In the following part we will explicitly refer to hybrid halide perovskites and show that their properties, at least under dark conditions, are very similar to the ones established for oxide mixed conductors.

3.1. First Indications. First indications of the presence of mobile ionic species in hybrid halide perovskites came from the observation of "anomalous" polarization phenomena in perovskite solar cells under operation. These behaviors appeared at long times (or low a.c. frequencies) in the form of hysteretic $i-V$ curves,[1−4] high apparent dielectric constants,[5,6] and field-switchable photovoltaic effects.[7] While initially some of these phenomena were attributed to ferroelectricity stemming from the organic cation dipoles,[64,65] this assessment was later revised due to the highly disordered nature of these dipoles at room temperature.[66−69] In fact the reported phenomena are strikingly similar to the stoichiometric polarization effects described in section 2.2.

An observation of ion migration in hybrid perovskites was already given in ref 7, albeit the changes reported appeared irreversible (or not clearly reversible). Similar evidence was later reported in refs 70 and 71. We find it important to stress here that these results have been observed under degradation conditions (see section 3.2), and as such are not directly representative of equilibrium properties (e.g., bulk ion conduction).

A direct measurement of reversible bulk ion conduction in MAPI, and its separation from the electronic response, was first reported in ref 8 using d.c. galvanostatic polarization and emf measurements under equilibrium conditions. This was later complemented by ref 72. It is also worth noting that several halide perovskites, both hybrid and fully inorganic, were already assessed as mixed conductors long before their application in photovoltaic devices.[73−76] Alongside these first experimental reports, consistent supporting evidence came from computational works indicating the ease of formation (and, in some cases, high mobility) of ionic defects in hybrid halide perovskites (in particular in MAPI).[77−82] Nonetheless, there is no good agreement on the predicted formation energies,[77,79] nor on the extracted activation energies for mobility (e.g., migration energy for iodine vacancy motion in MAPI ranges between 0.08 and 0.58 eV).[80−82]

3.2. Points of Concern in Electrochemical Characterizations. Here we discuss a few key aspects in the study of halide perovskites and of their ionic motion that we feel have not received adequate attention. These refer to the thermodynamic definition of the materials, the impact of voltage on stability as well as on ion diffusion, and the difficulty in measuring and evaluating activation energies.

As already mentioned, many experiments (usually electrical or electrochemical) aimed at clarifying ion motion in halide perovskites are not performed under reversible and defined conditions, casting doubts on the conclusions. First of all, the charge carrier thermodynamics requires (beside definition of pressure and temperature) definition of stoichiometry and doping content. A crucial role in this context is played by the halogen partial pressure (stoichiometry) and by the oxygen partial pressure (acceptor doping), which severely influence the charge carrier concentrations (section 2.1). Moreover, halide perovskites suffer from severe stability problems, which can be induced by temperature, water/humidity, oxygen, high-

DOI: 10.1021/jacs.8b13594
J. Am. Chem. Soc. 2019, 141, 8382−8396

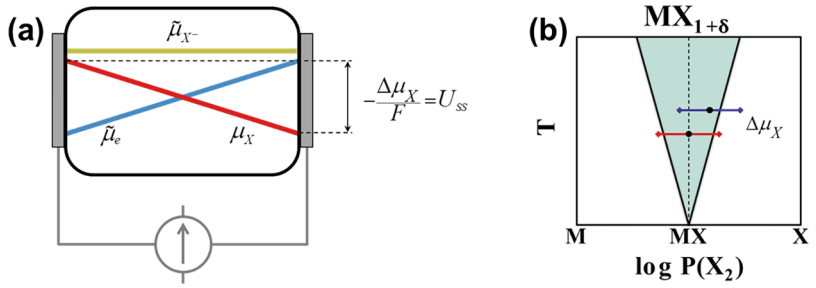

Figure 6. (a) Consequence of the application of a voltage to a mixed conductor with ion-blocking electrodes. Due to the nature of the contacts, in the steady state the chemical potential of the halide ions ($\tilde{\mu}_{X^-}$) is constant, while the electron and neutral halogen chemical potentials ($\tilde{\mu}_e$ and μ_X) follow the voltage and give rise to a stoichiometric polarization. (b) Stability window of a binary metal halide MX as a function of temperature, representing tolerable changes in stoichiometry (δ). Application of a voltage induces a variation in μ_X^*, which establishes on the two sides of a material chemical potential values which may exceed the stability window (red line). Depending on the initial position of the sample within the stability window, only one of the two chemical potential values may fall outside the window (blue line), but this occurrence still leads to degradation.

intensity light, or a combination thereof. Lack of control over these parameters can lead to rapid degradation and to the irreversible loss of volatile components, affecting the measurements.

Another very important—and almost entirely overlooked—source of instability can be voltage. In several experiments, a voltage is applied across two terminals to induce ion movement, while the migration is monitored by different methods. The reported voltages applied were usually very high, in the range of tens to hundreds of volts, and as such above the thermodynamically expected decomposition voltage. It is straightforward to connect this with the stoichiometric polarization discussed in section 2.2. Irrespective of the resulting electric field, the voltage—if applied by electrodes that block the ions—induces in the steady state (SS) a difference in the chemical potential of the components which may easily exceed the stability limit ($U_{SS} = -\Delta\mu_X/F$, as $\Delta\tilde{\mu}_{X^-} = 0$; see Figure 6a). Of particular relevance for halide perovskites is the chemical potential difference of the halogen ($\Delta\mu_X$), as this is the most mobile species (Figure 6). Already a voltage of 1.4 V suffices to drive $MAPbI_3$, $MAPbBr_3$, and $MAPbCl_3$ out of their stability range and to decompose them in methylamine, lead halides, and hydrogen halides even under standard conditions (standard Gibbs formation energies for this reaction are −125, −130, and −113 kJ/mol, respectively).[83] A voltage of 5.1 V is even enough to decompose $MAPbI_3$, $MAPbBr_3$, and $MAPbCl_3$ into elements (standard Gibbs energy of formation for this reaction are −260, −400, and −490 kJ/mol, respectively).[83] Under these conditions, eventually degradation will occur, starting from the electrode interfaces. In halide perovskites, the kinetics of these processes is rather quick, in particular under illumination, and as such a metastable situation is not expected (as it may be the case for materials with very low ionic conductivities).

Let us now discuss the effect of voltage on the ionic transport. As the migration thresholds for ion transport are usually of the order of 0.1 eV or higher, hopping kinetics show that the local ion conductivities are not affected by the voltage, unless the resulting electric field is relevant at the hopping distance, i.e. in the order of 0.1 V/nm.[41] Even with micrometer-size electrode spacing, the voltages required to reach such electric fields will exceed the decomposition voltage. A different question is the influence of voltage on local defect concentrations (mentioned in section 2.2), which stems from the bulk concentration polarization based on the coupling between voltage and chemical potential. As shown in Figure 4 for $SrTiO_3$, for voltages on the order of a few hundred volts (which is insufficient to induce the above-mentioned effect) the concentration variations can be sharp, but still describable by a (spatially dependent) chemical diffusion coefficient. While these voltages exceed the decomposition voltage, the very sluggish cation diffusion in this material, combined with the short application times of the voltage, allow for a metastable situation.

The last issue worth discussing here concerns activation energy measurements, which have been heavily used to characterize ionic mobility in halide perovskites and are often based on Arrhenius-type plots of the conductivity. Four points are worth mentioning: (i) In mixed conductors, it is not adequate to speak of an activation energy for the total conductivity. Rather, the T-dependences for the various species have to be considered separately, as the materials can be equally ionically and electronically conducting, especially under equilibrium conditions.[8,72] (ii) It cannot be assumed that, upon varying temperature, the charge carrier concentrations will remain constant. This stems not only from possible irreversibility effects such as loss of extrinsic (oxygen, residual solvent molecules, etc.) or even intrinsic components (methylamine, halogen), but also from the fact that the conductivity activation energy contains a defect formation term alongside the mobility term. (iii) At the expected relatively high defect concentrations and low temperatures, defect association may heavily impact the activation energy value. Upon heating, dissociation of defect complexes (ionic−ionic or ionic−electronic) would give rise to an effectively enhanced free carrier concentration, yielding even higher activation energies. A further complication, as discussed in ref 84, deals with the simultaneous presence of intrinsic and extrinsic defect regimes which can be crossed as a function of temperature. (iv) The best defined situation as far as measurement and evaluation are concerned is when the T-dependence is studied at constant halide partial pressure (E_P). This requires reversible electrodes and possibly very long equilibration times. The alternative is to measure at constant stoichiometry (i.e., in a sealed system), so to assess a different—but related—value of the activation energy (E_δ). According to $\sigma(\delta,T) = \sigma(P_{X_2}(\delta,T), T)$, E_δ can then be related to E_P through the following equation:[85]

DOI: 10.1021/jacs.8b13594
J. Am. Chem. Soc. 2019, 141, 8382−8396

$$E_\delta - E_P = -\left(\frac{\partial \ln \sigma}{\partial \ln(P(X_2))}\right)_T \left(R\frac{\partial \ln(P(X_2))}{\partial 1/T}\right)_\delta \quad (14)$$

If these conditions are not guaranteed, then the meaning of the temperature dependence is complex.

3.3. The Nature of Ion Conduction under Equilibrium Conditions. A significant amount of work has been dedicated to unraveling the nature of ion conduction in hybrid halide perovskites. Unsurprisingly, most of the works focused on MAPI. In general, almost all the contributions identify either iodide ions[8,12,15,86−90] and/or methylammonium ions[70,71,89−92] to be mobile. Extrinsic ion migration (Li, Au) has been studied as well.[93−95] Unfortunately, many of the reports lacked unambiguous and/or direct experimental evidence (see also previous section), causing the question on the nature of ion conduction in these materials to remain open for a surprisingly long time.

Direct experimental evidence comes from reaction cell experiments, where a significant iodine diffusion in MAPI is observed in the form of secondary phase formation (Figure 7).[8,72] While these experiments cannot rule out a parallel minor diffusion of the cations, they clearly demonstrate iodine motion as a major contribution. This occurrence is entirely unsurprising, as fast and reversible halide exchange (for which halide diffusion is necessary) was observed for halide perovskites,[96−98] in agreement with earlier works reporting halide conduction in several halide perovskites.[73−76] Note also that the perovskite structure favors anion transport, as extensively shown for oxide ion conduction in oxide perovskites.

As far as the cation diffusion is concerned, all previous observations are either indirect or irreversible (often simultaneous with phase degradation). An example is reported in Figure 8, where MA ions in MAPI migrate under illumination and bias, leading to phase degradation close to the electrodes. While this process is surely relevant for the material (and device) stability, it is not the one we are interested in when it comes to bulk charge transport in materials and devices.

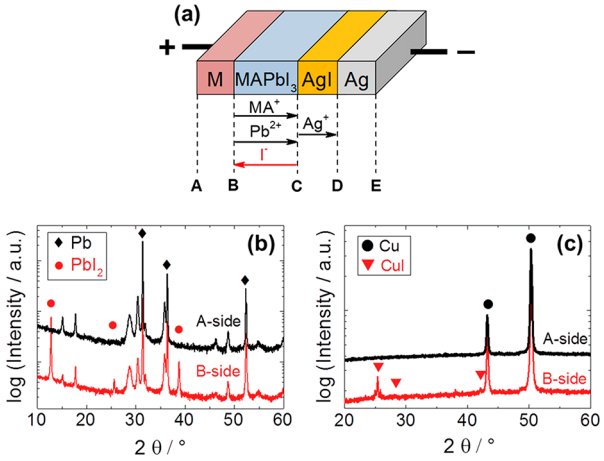

Figure 7. Faradaic reaction cell experiments in the dark. (a) Schematics of the cell +M|MAPI|AgI|Ag−, with M = Cu or Pb. (b) XRD analysis of the interfaces of the reaction cell with M = Pb, after flowing 50 nA/cm^2 of current for 1 week at 343 K under Ar atmosphere. Note the formation of PbI_2 at the Pb|MAPI contact. No other secondary phases were present at any other interface, and no PbI_2 formation was observed in the absence of current flow.[8,72] (c) XRD analysis of the interfaces of the reaction cell with M = Cu, after flowing 25 nA/cm^2 of current for 1 week at 323 K under Ar atmosphere. Note the formation of CuI at the Cu|MAPI contact. No other secondary phases were present at any other interface, and no CuI formation was observed in the absence of current flow.[8,72] Figure taken from ref 72, published 2017 under a Creative Commons license.

To reliably determine whether cation diffusion contributes to bulk charge transport, non-destructive and direct methods are required. Powerful tools in this respect are NMR and tracer diffusion experiments. As shown in Figure 9, ^{1}H NMR spectra present a large, almost invariant line width as a function of temperature, which indicate absence of significant MA diffusion.[72] ^{14}N spectra, given in Figure 9a, consistently show a typical quadrupolar splitting in the tetragonal phase of MAPI that could only exist without significant isotropic motion (e.g., diffusion). The results are in agreement with tracer diffusion experiments, where only a negligible MA diffusion is observed (orders of magnitude below the iodine transport).[72,99] Similar conclusions can be drawn for Pb cations based on the quasi-invariance of the ^{207}Pb line width with temperature (Figure 9c). Based on the above evidence it is clear that, at least for equilibrium conditions, only iodide ions are sufficiently mobile as to be relevant for the macroscopic charge transport. Nonetheless, a minor diffusivity of the cations (as directly observed for MA)[72,99] is still expected to be of importance for decomposition processes and cation exchange reactions.[100,101]

The remaining question to be addressed is then related to the defect mechanism behind the iodine transport (vacancy- or interstitial-based). In oxide perovskites, interstitial oxide motion can be excluded owing to site and bond arguments. Most of the existing computational literature on halide perovskites also suggests that halide vacancies have lower activation energies for the motion,[80−82] but in some cases interstitials appear equally mobile.[82] Normally, due to the high density of the structure, Schottky disorder is much more common than anti-Frenkel disorder (halide displacement from a regular lattice site, forming a vacancy and an interstitial) in perovskites. Moreover, as already mentioned, many oxide perovskites are oxide-ion (or proton) conductors via oxygen vacancies. To identify the dominant ionic defects in MAPI and halide perovskites, one can apply solid-state ionic approaches such as the one described previously. As shown in Figure 10a−c, defect chemical modeling at the level of mass action laws (see section 2.1) can be used to predict the effects of stoichiometry changes, doping content, and oxygen incorporation on the defect concentrations.[46] These models can be compared with experiments, where stoichiometry variations, purposeful doping, and oxygen treatments are realized (Figure 10d−f) and the induced changes in ionic and electronic conductivities are recorded. The strong and reversible enhancement of electronic conductivity upon increase in the iodine partial pressure unambiguously indicates electron holes as the dominant electronic carriers (cf. Figure 10a,d). This is consistent with the doping experiment of Figure 10e, where acceptor doping clearly increases the electronic conductivity (cf. Figure 10b). Note that, according to the defect chemical modeling, we also expect a transition from p- to n-type electronic conductivity at sufficiently low $P(I_2)$ (see N region of Figure 10a). This occurrence is indeed experimentally observed when exposing the samples to an I_2 sink.[37] As far as the ionic conductivity is concerned, as shown in Figure 10d this reversibly decreases as a function of $P(I_2)$, indicating iodine vacancies as dominant ionic charge carriers, as these are

DOI: 10.1021/jacs.8b13594
J. Am. Chem. Soc. 2019, 141, 8382−8396

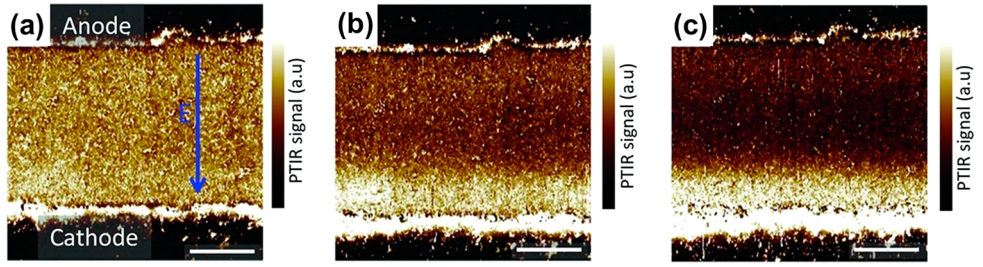

Figure 8. Photothermal induced resonance (PTIR) microscopy of MAPI thin film under 80 V (1.6 V/μm) of bias: (a) before applying bias, (b) after 100 s, and (c) after 200 s. Scale bars are 20 μm. Bright area represents MA accumulation. Adapted with permission from ref 70.

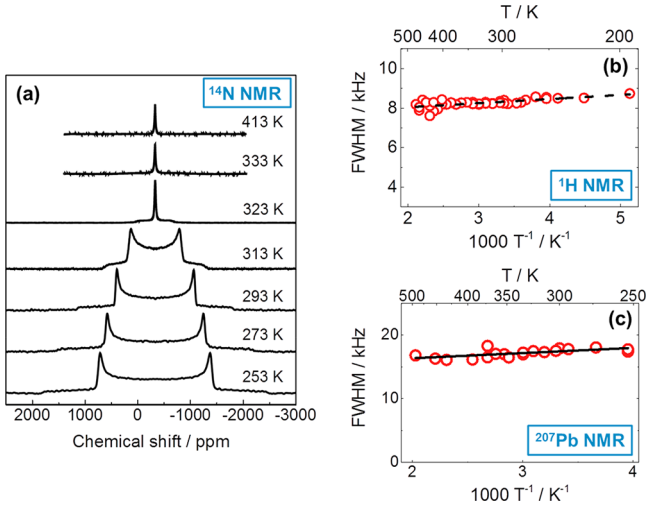

Figure 9. NMR analysis of cation diffusion in MAPI. (a) ^{14}N spectra displaying a quadrupolar splitting at T < 323 K (tetragonal phase). The existence of such splitting necessarily indicates absence of significant isotropic motion in this phase. (b) Full width at half-maximum of ^{1}H NMR spectra as a function of temperature. The line width does not significantly vary with T and remains large even at 500 K, indicating lack of cation diffusion (this motion would average the intermolecular dipole−dipole interaction composing the line width that are not averaged by internal rotation).[69,72] (c) Full width at half-maximum of ^{207}Pb NMR spectra as a function of temperature. The same arguments used for the proton case of panel (b) are valid here. Figure taken from ref 72, published 2017 under a Creative Commons license.

annealed by iodine incorporation (see eq 6). We note here that the comparable changes of σ_{ion} and σ_{eon} on a logarithmic scale would also indicate not too dissimilar concentrations of the relevant charge carriers (see defect diagram of Figure 10a, I-to-P transition regime). This is in contrast with conductivity experiments showing comparable ionic and electronic conductivities in these samples, and as such it remains an open question. A more detailed account of this discrepancy has been given in ref 46. Nevertheless, the increase of ionic conductivity upon acceptor doping given in Figure 10e strongly confirms iodine vacancies to be the dominant ionic charge carriers.[46,72] In addition, as shown in Figure 10f, the increase in ionic and electronic conductivity upon O_2 incorporation (expected to behave as acceptor dopant if incorporated sufficiently, see Figure 10c) provides a further confirmation of the nature of the dominant carriers. This defect chemical approach clearly reveals that, in MAPI, iodine vacancies are the dominant ionic (and electron holes the dominant electronic) charge carriers under equilibrium conditions.[33,46,72]

Nonetheless, there are reports on iodine interstitials being dominant charge carriers,[84] with experimental evidence for mobile interstitials claimed in refs 24 and 28. In ref 24, both iodide vacancies and interstitials are proposed using results of activation energy values, which are, however, debatable (see section 3.2). In ref 28, neutron scattering experiments reveal the presence of iodine interstitials, which are claimed to form neutral I_2 molecules. Changes in occupancy between regular and interstitial sites are used to infer migration, even though they are more representative of an interstitial formation process, as migration involves a jump from an interstitial site to another. The observation of interstitial neutral iodine is consistent with the much smaller size with respect to an iodide ion, and this aspect is also discussed in the mechanism of light-enhanced ionic conductivity (see section 3.4).[37] In this respect, it is still questionable whether the dominant defect disorder in this material is of Schottky ($[V'_{MA}] = [V_I^{\bullet}]$) or anti-Frenkel ($[V_I^{\bullet}] = [I'_i]$) type, as in both cases the iodide vacancy concentration would be predominant. Experimental results given in ref 28 suggest the presence of anti-Frenkel disorder, while indication of Schottky disorder is found in the observation of a perceptible (albeit minor) MA diffusion,[72,99] which is consistent with the presence of a high concentration of MA defects (e.g., vacancies). Without further evidence, none of the above can be taken as a conclusive result. Importantly, the low temperature situation in halide perovskites (e.g., around room temperature) is very likely an extrinsic situation dominated by impurities (e.g., oxygen, metal ions, etc.) compensating for $V_I^{\bullet}$. This assessment is based on the comparatively low native point defect concentrations with respect to the expected impurity level (coming, e.g., from the solution-based synthesis) and also on all the experience on oxide perovskites at low temperatures. A similar evaluation was also proposed in ref 84.

As a final note, we want to stress the importance of interfacial redistribution phenomena for these materials, both at grain boundaries and at hetero-interfaces. Ongoing work already shows that equilibrium space charge polarization in halide perovskites under equilibrium is, to a significant extent, ionically controlled.[102] Such behavior could indeed be expected based on the higher concentration of ionic charge carriers. This redistribution may have important consequences for the charge-transfer and recombination phenomena taking place at the interfaces in working devices, and as such deserves a thorough investigation. A recent example of a study of the effect of ionic carrier redistribution on charge transfer in photovoltaic devices is given in ref 20.

3.4. Light Effects on Ion Conduction. Having understood the mixed conducting transport in the dark, we can now move to consider the situation under illumination. The various

DOI: 10.1021/jacs.8b13594
J. Am. Chem. Soc. 2019, 141, 8382−8396

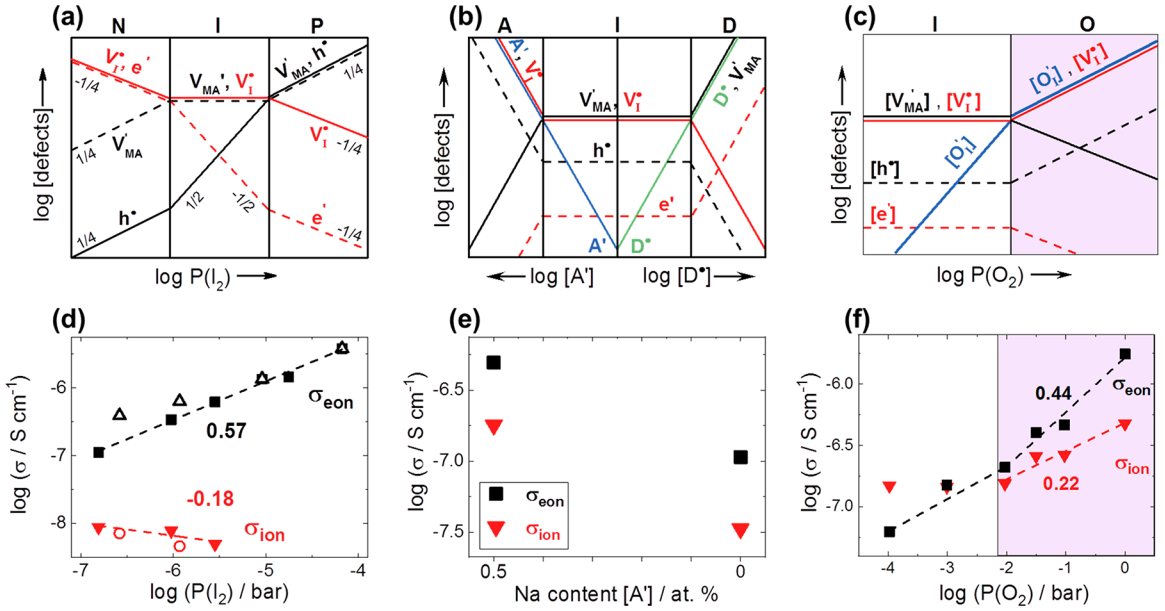

Figure 10. (a–c) Defect chemical modeling applied to MAPI to reveal the defect concentrations dependences as a function of (a) stoichiometry (iodine partial pressure), (b) acceptor and donor doping content, and (c) oxygen partial pressure. (d–f) Ionic and electronic conductivity of MAPI as a function of (d) iodine partial pressure (Ar as carrier gas), (e) acceptor (Na) dopant content (under Ar and 2×10^{-7} bar I_2), and (f) oxygen partial pressure (Ar as carrier). The $P(O_2)$ dependence is measured in a thin film kept at 333 K under weak illumination (0.5 mW/cm^2) to accelerate the incorporation kinetics.[33] All the other samples are pellets measured using d.c. galvanostatic polarization at 343 K in the dark. Figures taken from refs 33, 46, and 72, all published under Creative Commons licenses.

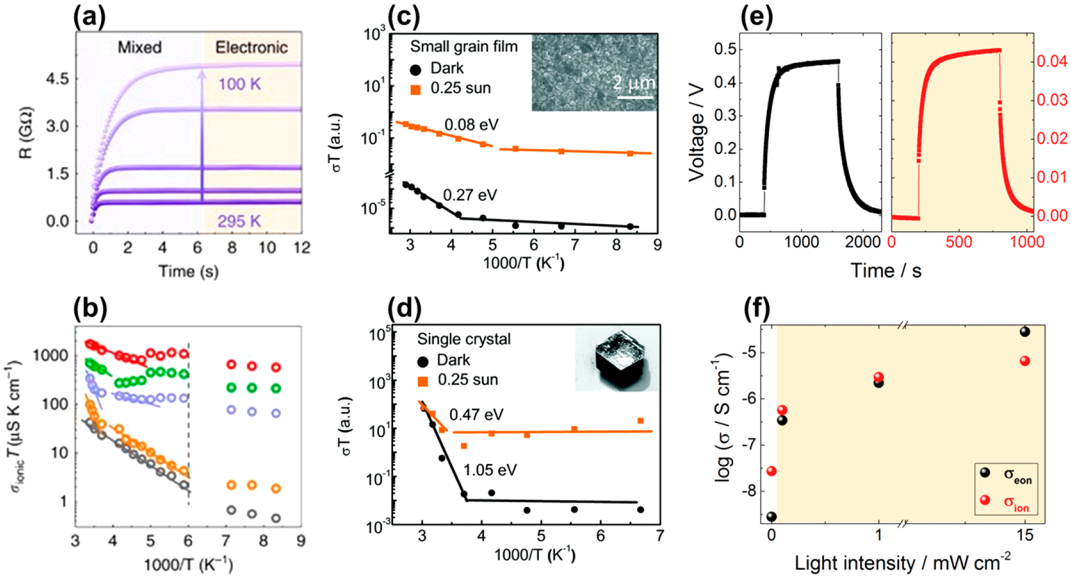

Figure 11. (a, b) Direct current polarization experiments on MAPI thin films under illumination as a function of temperature: (a) d.c. polarization curves under 1 mW/cm^2 light and (b) extracted values for ionic conductivity under several light intensities (from 0 mW/cm^2 in gray symbols to 20 mW/cm^2 in red symbols). Adapted from ref 104. Published 2016 under a Creative Commons license. (c, d) Activation energy of the total electrical conductivity of MAPI (c) thin films and (d) single crystals as a function of temperature and illumination. Figure from ref 103, reproduced by permission of the PCCP Owner Societies. (e, f) D.c. polarization experiments on MAPI thin films as a function of light intensity at 313 K: (e) d.c. polarization curves in the dark (black) and under 1 mW/cm^2 light (red) and (f) extracted values for ionic and electronic conductivity. Figures (e) and (f) first published in ref 37.

indications for ion transport discussed earlier were already collected under illumination and in working photovoltaic devices,[1−7] suggesting the relevance of the ionic transport even under light. Interestingly, this would imply light-induced changes of the ionic transport itself happening alongside the electronic excitation. Indeed, light effects on bulk ionic transport in freestanding halide perovskites were suggested in refs 8, 103, and 104. Figure 11 shows such light effects on d.c. polarization curves or on the effective conductivity activation barriers. Note that the latter measurement is sensitive to the total conductivity and is also affected by defect formation and, even more importantly, defect association processes which have strong temperature dependences (see section 3.2).

DOI: 10.1021/jacs.8b13594
J. Am. Chem. Soc. 2019, 141, 8382−8396

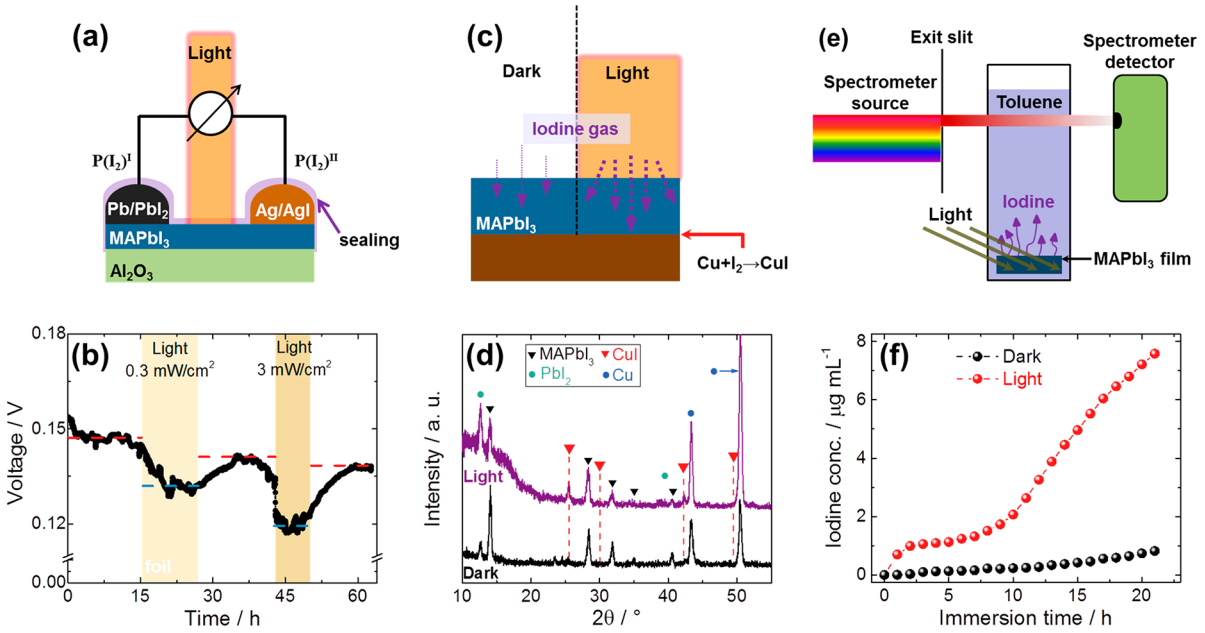

Figure 12. (a, b) Emf cell built on a MAPI thin film. Pb/PbI_2 and Ag/AgI mixtures are used as electrode and to provide a constant I_2 activity: (a) schematic and (b) voltage measured across the cell with and without light. The presence of a significant voltage under light necessarily means that a substantial portion of the conductivity is still ionic. (c, d) Permeation cell obtained by depositing a MAPI thin film on a Cu substrate and exposing it to I_2 vapor: (c) schematic and (d) formation of CuI on the illuminated side probed by XRD. The formation of CuI solely on the illuminated side indicates an enhanced permeation flux, consistent with higher ion conduction under light. (e, f) Excorporation experiment performed by immersing a MAPI film in toluene: (e) schematic and (f) concentration of I_2 excorporated into toluene as a function of time, with and without 1 mW/cm^2 illumination. The accelerated iodine loss under illumination indicates enhanced iodine transport. Figures first published in ref 37.

Even though the ion conduction enhancement is strongly corroborated by the detailed analysis of the polarization transients,[37] these experiments are not sufficient to unambiguously confirm the mixed conducting nature of a sample (as already discussed in section 2.2). To exclude electronic effects as the cause for these observations, more direct experimental methods are required, such as emf cells, permeation cells, and excorporation experiments.[37] As shown in Figure 12, these characterizations consistently show the presence of ionic conduction in MAPI even under illumination. Moreover, they indicate that an enhanced iodine transport is taking place.[37] To understand the nature of the dominant charge carriers under light, tracer diffusion and NMR experiments were carried out on thin films under light,[99] in addition to stoichiometric variations and Hall effect measurements.[37] The qualitative charge carrier situation turned out to be similar to the dark case, at least for low light intensities. As in the dark, electron holes and iodine vacancies appear to be the dominant ionic and electronic charge carriers.

Based on this knowledge, a mechanism for the photoinduced enhancement of ion transport was proposed in ref 37. It relies on the interaction of electron holes with iodide ions sitting on regular iodine sites. Irrespective of the role of excess electrons, the holes can be localized neutralizing negatively charged iodide ions. These neutral atoms, due to a significantly lower size and to the tendency to interact with iodide ions in order to share the charge, can easily be displaced (e.g., interstitially), leaving an iodine vacancy behind, which is enabling the enhanced ion transport. Note that self-trapping processes involving electron holes and halide ions, and also the formation of halide dimers sharing a single negative charge (but not the increased σ_{ion}) are very well known to happen in alkali halides.[105−108] This tentative mechanism would also have important implications for the photostability of MAPI (and possibly of other halide perovskites), as the enhanced ionic carrier concentration comes as a consequence of the formation of neutral iodine atoms. As such, this gives a heightened chemical potential of neutral iodine inside the perovskite material, which can act as the driving force for an irreversible loss of iodine under prolonged illumination in favor of a sink (e.g., toluene, vacuum, or the ambient gas phase).[37] As such processes would happen in bromides and iodides to a very different degree, this mechanism would also provide a straightforward explanation for the photoinduced phase separation of mixed iodide−bromide halide perovskites.[109] The different reactions of Br^- and I^- with electron holes would enhance the energy of the mixtures, in particular at comparable Br/I contents, favoring the formation of iodine-rich and bromine-rich domains. Lastly, as the described photoeffects are inherently connected with volume changes they may also be related to the macroscopic volume expansion observed in MAPI upon illumination.[110] At this stage, more experimental evidence is required to support these claims.

4. CONCLUSIONS AND OUTLOOK

So far, the equilibrium situation appears to be quite clear, and—from a solid-state ionics perspective—not at all unexpected. As in many oxide perovskites, we are dealing here with a mixed conducting material in which the majority of the ionic transport is carried by anion vacancies. Moreover, the behavior observed (particularly under equilibrium conditions) upon stoichiometry changes and the occurrence of stoichiometric polarization both conform to the expected behavior of a typical oxide perovskite. Similarities may also be expected regarding the impact of higher-dimensional defects on the point defect concentrations. Due to the soft structure of these

DOI: 10.1021/jacs.8b13594
J. Am. Chem. Soc. 2019, 141, 8382−8396

materials, and to their practical use in contact with other phases, this latter aspect should be worth investigating in detail.

In contrast, major differences with the high temperature situation in oxide perovskites lie in (i) the expected high degree of defect association due to low temperature (and high defect concentrations), (ii) a more important role of impurities (or frozen-in native defects) as compensating majority defects, and (iii) the significant light effects on ionic transport. While the first points stem from the different temperature regimes but are not rooted in a different underlying charge carrier chemistry, the third point is surprising and can be ascribed to the less dense structure of MAPI as compared to, e.g., $SrTiO_3$. Concerning the first point, defect concentrations and mobility values still remain to be unambiguously determined, both in the dark and under illumination. This aspect extends to the halide perovskite compositions used in devices (e.g., mixed-cation and mixed-anion) and would greatly help quantitatively understanding the charge transport in these materials. Regarding the second point, it would be important to identify and quantify the possible impurities present in these materials, so to assess their impact on the properties of materials and devices. As to the third point, the atomistic mechanism of the photoenhancement remains to be clearly proven, and the connection to the stability of the materials deserves special attention. Of particular interest may be the relation between the photoenhanced ion conduction and the halide demixing in mixed-anion compositions, as well as the potential effect on the phase volume. In the context of this Perspective, the most important issues for the future are (i) to evaluate the application of the solid-state ionics toolbox to the function of halide perovskite-based photovoltaic devices, in terms of bulk as well as interfacial defect chemistry, and (ii) to explore the consequences of the photoenhanced ion conduction regarding novel light-triggered or light-sensitive devices.

AUTHOR INFORMATION

Corresponding Author

*alessandro.senocrate@googlemail.com

ORCID

Alessandro Senocrate: 0000-0002-0952-0948

Joachim Maier: 0000-0003-2274-6068

Notes

The authors declare no competing financial interest.

ACKNOWLEDGMENTS

The authors are grateful to Dr. Gee Yeong Kim, Dr. Davide Moia, and Dr. Rotraut Merkle for helpful discussions. The collaboration with Michael Grätzel and his group at EPFL (Lausanne, CH) is gratefully acknowledged.

REFERENCES

(1) Dualeh, A.; Moehl, T.; Tétreault, N.; Teuscher, J.; Gao, P.; Nazeeruddin, M. K.; Grätzel, M. Impedance Spectroscopic Analysis of Lead Iodide Perovskite-Sensitized Solid-State Solar Cells. *ACS Nano* **2014**, *8* (1), 362−373.

(2) Snaith, H. J.; Abate, A.; Ball, J. M.; Eperon, G. E.; Leijtens, T.; Noel, N. K.; Stranks, S. D.; Wang, J. T.-W.; Wojciechowski, K.; Zhang, W. Anomalous Hysteresis in Perovskite Solar Cells. *J. Phys. Chem. Lett.* **2014**, *5* (9), 1511−1515.

(3) Jeon, N. J.; Noh, J. H.; Kim, Y. C.; Yang, W. S.; Ryu, S.; Seok, S. I. L. Solvent Engineering for High-Performance Inorganic-Organic Hybrid Perovskite Solar Cells. *Nat. Mater.* **2014**, *13* (9), 897−903.

(4) Unger, E. L.; Hoke, E. T.; Bailie, C. D.; Nguyen, W. H.; Bowring, A. R.; Heumüller, T.; Christoforo, M. G.; McGehee, M. D. Hysteresis and Transient Behavior in Current-voltage Measurements of Hybrid-Perovskite Absorber Solar Cells. *Energy Environ. Sci.* **2014**, *7* (11), 3690−3698.

(5) Juarez-Perez, E. J.; Sanchez, R. S.; Badia, L.; Garcia-Belmonte, G.; Kang, Y. S.; Mora-Sero, I.; Bisquert, J. Photoinduced Giant Dielectric Constant in Lead Halide Perovskite Solar Cells. *J. Phys. Chem. Lett.* **2014**, *5* (13), 2390−2394.

(6) Sanchez, R. S.; Gonzalez-Pedro, V.; Lee, J.-W.; Park, N.-G.; Kang, Y. S.; Mora-Sero, I.; Bisquert, J. Slow Dynamic Processes in Lead Halide Perovskite Solar Cells. Characteristic Times and Hysteresis. *J. Phys. Chem. Lett.* **2014**, *5* (13), 2357−2363.

(7) Xiao, Z.; Yuan, Y.; Shao, Y.; Wang, Q.; Dong, Q.; Bi, C.; Sharma, P.; Gruverman, A.; Huang, J. Giant Switchable Photovoltaic Effect in Organometal Trihalide Perovskite Devices. *Nat. Mater.* **2015**, *14* (2), 193−198.

(8) Yang, T.-Y.; Gregori, G.; Pellet, N.; Grätzel, M.; Maier, J. The Significance of Ion Conduction in a Hybrid Organic-Inorganic Lead-Iodide-Based Perovskite Photosensitizer. *Angew. Chem., Int. Ed.* **2015**, *54* (27), 7905−7910.

(9) Lopez-Varo, P.; Jiménez-Tejada, J. A.; García-Rosell, M.; Anta, J. A.; Ravishankar, S.; Bou, A.; Bisquert, J. Effects of Ion Distributions on Charge Collection in Perovskite Solar Cells. *ACS Energy Lett.* **2017**, *2* (6), 1450−1453.

(10) Kim, S.; Bae, S.; Lee, S.-W.; Cho, K.; Lee, K. D.; Kim, H.; Park, S.; Kwon, G.; Ahn, S.-W.; Lee, H.-M.; et al. Relationship between Ion Migration and Interfacial Degradation of $CH_3NH_3PbI_3$ Perovskite Solar Cells under Thermal Conditions. *Sci. Rep.* **2017**, *7* (1), 1200.

(11) Dhar, J.; Sil, S.; Dey, A.; Sanyal, D.; Ray, P. P. Investigation of Ion-Mediated Charge Transport in Methylammonium Lead Iodide Perovskite. *J. Phys. Chem. C* **2017**, *121* (10), 5515−5522.

(12) Li, C.; Tscheuschner, S.; Paulus, F.; Hopkinson, P. E.; Kießling, J.; Köhler, A.; Vaynzof, Y.; Huettner, S. Iodine Migration and Its Effect on Hysteresis in Perovskite Solar Cells. *Adv. Mater.* **2016**, *28* (12), 2446−2454.

(13) Chen, S.; Wen, X.; Sheng, R.; Huang, S.; Deng, X.; Green, M. A.; Ho-Baillie, A. Mobile Ion Induced Slow Carrier Dynamics in Organic-Inorganic Perovskite $CH_3NH_3PbBr_3$. *ACS Appl. Mater. Interfaces* **2016**, *8* (8), 5351−5357.

(14) Meloni, S.; Moehl, T.; Tress, W.; Franckevičius, M.; Saliba, M.; Lee, Y. H.; Gao, P.; Nazeeruddin, M. K.; Zakeeruddin, S. M.; Rothlisberger, U.; et al. Ionic Polarization-Induced Current-voltage Hysteresis in $CH_3NH_3PbX_3$ Perovskite Solar Cells. *Nat. Commun.* **2016**, *7*, 10334.

(15) De Bastiani, M.; Dell'Erba, G.; Gandini, M.; D'Innocenzo, V.; Neutzner, S.; Kandada, A. R. S.; Grancini, G.; Binda, M.; Prato, M.; Ball, J. M.; et al. Ion Migration and the Role of Preconditioning Cycles in the Stabilization of the J - V Characteristics of Inverted Hybrid Perovskite Solar Cells. *Adv. Energy Mater.* **2016**, *6* (2), 1501453.

(16) Chen, B.; Yang, M.; Zheng, X.; Wu, C.; Li, W.; Yan, Y.; Bisquert, J.; Garcia-Belmonte, G.; Zhu, K.; Priya, S. Impact of Capacitive Effect and Ion Migration on the Hysteretic Behavior of Perovskite Solar Cells. *J. Phys. Chem. Lett.* **2015**, *6* (23), 4693−4700.

(17) Zhao, Y.; Liang, C.; Zhang, H.; Li, D.; Tian, D.; Li, G.; Jing, X.; Zhang, W.; Xiao, W.; Liu, Q.; et al. Anomalously Large Interface Charge in Polarity-Switchable Photovoltaic Devices: An Indication of Mobile Ions in Organic-Inorganic Halide Perovskites. *Energy Environ. Sci.* **2015**, *8* (4), 1256−1260.

(18) Game, O. S.; Buchsbaum, G. J.; Zhou, Y.; Padture, N. P.; Kingon, A. I. Ions Matter: Description of the Anomalous Electronic Behavior in Methylammonium Lead Halide Perovskite Devices. *Adv. Funct. Mater.* **2017**, *27* (16), 1606584.

(19) Li, D.; Wu, H.; Cheng, H.-C.; Wang, G.; Huang, Y.; Duan, X. Electronic and Ionic Transport Dynamics in Organolead Halide Perovskites. *ACS Nano* **2016**, *10* (7), 6933−6941.

(20) Moia, D.; Gelmetti, I.; Calado, P.; Fisher, W.; Stringer, M.; Game, O.; Hu, Y.; Docampo, P.; Lidzey, D.; Palomares, E. Ionic-to-

DOI: 10.1021/jacs.8b13594
J. Am. Chem. Soc. 2019, 141, 8382−8396

Electronic Current Amplification in Hybrid Perovskite Solar Cells: Ionically Gated Transistor-Interface Circuit Model Explains Hysteresis and Impedance of Mixed Conducting Devices. *Energy Environ. Sci.* **2019**, *12* (4), 1296−1308.
(21) Li, W.; Rothmann, M. U.; Liu, A.; Wang, Z.; Zhang, Y.; Pascoe, A. R.; Lu, J.; Jiang, L.; Chen, Y.; Huang, F.; et al. Phase Segregation Enhanced Ion Movement in Efficient Inorganic $CsPbIBr_2$ Solar Cells. *Adv. Energy Mater.* **2017**, *7* (20), 1700946.
(22) Hoque, M. N. F.; Islam, N.; Li, Z.; Ren, G.; Zhu, K.; Fan, Z. Ionic and Optical Properties of Methylammonium Lead Iodide Perovskite across the Tetragonal-Cubic Structural Phase Transition. *ChemSusChem* **2016**, *9* (18), 2692−2698.
(23) Zhang, Y.; Liu, M.; Eperon, G. E.; Leijtens, T. C.; McMeekin, D.; Saliba, M.; Zhang, W.; de Bastiani, M.; Petrozza, A.; Herz, L. M.; et al. Charge Selective Contacts, Mobile Ions and Anomalous Hysteresis in Organic-Inorganic Perovskite Solar Cells. *Mater. Horiz.* **2015**, *2* (3), 315−322.
(24) Birkhold, S. T.; Precht, J. T.; Giridharagopal, R.; Eperon, G. E.; Schmidt-Mende, L.; Ginger, D. S. Direct Observation and Quantitative Analysis of Mobile Frenkel Defects in Metal Halide Perovskites Using Scanning Kelvin Probe Microscopy. *J. Phys. Chem. C* **2018**, *122* (24), 12633−12639.
(25) Walter, D.; Fell, A.; Wu, Y.; Duong, T.; Barugkin, C.; Wu, N.; White, T. P.; Weber, K. Transient Photovoltage in Perovskite Solar Cells: Interaction of Trap-Mediated Recombination and Migration of Multiple Ionic Species. *J. Phys. Chem. C* **2018**, *122*, 11270−11281.
(26) Zohar, A.; Levine, I.; Gupta, S.; Davidson, O.; Azulay, D.; Millo, O.; Balberg, I.; Hodes, G.; Cahen, D. What Is the Mechanism of $MAPbI_3$ P-Doping by I_2? Insights from Optoelectronic Properties. *ACS Energy Lett.* **2017**, *2* (10), 2408−2414.
(27) Liu, J.; Yin, X.; Liu, X.; Que, M.; Que, W. Multi-Influences of Ionic Migration on Illumination-Dependent Electrical Performances of Inverted Perovskite Solar Cells. *J. Phys. Chem. C* **2017**, *121* (29), 16051−16057.
(28) Minns, J. L.; Zajdel, P.; Chernyshov, D.; van Beek, W.; Green, M. A. Structure and Interstitial Iodide Migration in Hybrid Perovskite Methylammonium Lead Iodide. *Nat. Commun.* **2017**, *8*, 15152.
(29) Lee, H.; Gaiaschi, S.; Chapon, P.; Marronnier, A.; Lee, H.; Vanel, J.-C.; Tondelier, D.; Bourée, J.-E.; Bonnassieux, Y.; Geffroy, B. Direct Experimental Evidence of Halide Ionic Migration under Bias in $CH_3NH_3PbI_{3-x}Cl_x$ -Based Perovskite Solar Cells Using GD-OES Analysis. *ACS Energy Lett.* **2017**, *2* (4), 943−949.
(30) Cheng, Y.; Li, H.-W.; Qing, J.; Yang, Q.-D.; Guan, Z.; Liu, C.; Cheung, S. H.; So, S. K.; Lee, C.-S.; Tsang, S.-W. The Detrimental Effect of Excess Mobile Ions in Planar $CH_3NH_3PbI_3$ Perovskite Solar Cells. *J. Mater. Chem. A* **2016**, *4* (33), 12748−12755.
(31) Bag, M.; Renna, L. A.; Adhikari, R. Y.; Karak, S.; Liu, F.; Lahti, P. M.; Russell, T. P.; Tuominen, M. T.; Venkataraman, D. Kinetics of Ion Transport in Perovskite Active Layers and Its Implications for Active Layer Stability. *J. Am. Chem. Soc.* **2015**, *137* (40), 13130−13137.
(32) Carrillo, J.; Guerrero, A.; Rahimnejad, S.; Almora, O.; Zarazua, I.; Mas-Marza, E.; Bisquert, J.; Garcia-Belmonte, G. Ionic Reactivity at Contacts and Aging of Methylammonium Lead Triiodide Perovskite Solar Cells. *Adv. Energy Mater.* **2016**, *6* (9), 1502246.
(33) Senocrate, A.; Acartürk, T.; Kim, G. Y.; Merkle, R.; Starke, U.; Grätzel, M.; Maier, J. Interaction of Oxygen with Halide Perovskites. *J. Mater. Chem. A* **2018**, *6* (23), 10847−10855.
(34) Jamnik, J.; Maier, J. Transport across Boundary Layers in Ionic Crystals Part I: General Formalism and Conception. *Berichte der Bunsengesellschaft für Phys. Chemie* **1997**, *101* (1), 23−40.
(35) Riess, I.; Leshem, A. Odd Rectification, Hysteresis and Quasi Switching in Solid State Devices Based on Mixed Ionic Electronic Conductors. *Solid State Ionics* **2012**, *225*, 161−165.
(36) Maier, J. Ionic Conduction in Space Charge Regions. *Prog. Solid State Chem.* **1995**, *23* (3), 171−263.
(37) Kim, G. Y.; Senocrate, A.; Yang, T.-Y.; Gregori, G.; Grätzel, M.; Maier, J. Large Tunable Photoeffect on Ion Conduction in Halide Perovskites and Implications for Photodecomposition. *Nat. Mater.* **2018**, *17* (5), 445−449.
(38) Wagner, K. W.; Schottky, W. Theory of Controlled Mixed Phases. *Z. Phys. Chem.* **1930**, *11B*, 163.
(39) Kröger, F. A. *The Chemistry of Imperfect Crystals*; North-Holland Publishing Company: Amsterdam, 1964.
(40) Kofstad, P. *Nonstoichiometry, Diffusion, and Electrical Conductivity in Binary Metal Oxides*; Wiley-VCH Verlag, 1972.
(41) Maier, J. *Physical Chemistry of Ionic Materials*; John Wiley & Sons, Ltd: Chichester, UK, 2004.
(42) Heyne, L. Electrochemistry of Mixed Ionic-Electronic Conductors. In *Solid Electrolytes*; Geller, S., Ed.; Springer: Berlin/Heidelberg, 1977; pp 169−221.
(43) Merkle, R.; Maier, J. How Is Oxygen Incorporated into Oxides? A Comprehensive Kinetic Study of a Simple Solid-State Reaction with $SrTiO_3$ as a Model Material. *Angew. Chem., Int. Ed.* **2008**, *47* (21), 3874−3894.
(44) Maier, J. Complex Oxides: High Temperature Defect Chemistry vs. Low Temperature Defect Chemistry. *Phys. Chem. Chem. Phys.* **2003**, *5* (11), 2164−2173.
(45) Shi, T.; Chen, Y.; Guo, X. Defect Chemistry of Alkaline Earth Metal (Sr/Ba) Titanates. *Prog. Mater. Sci.* **2016**, *80*, 77−132.
(46) Senocrate, A.; Yang, T.-Y.; Gregori, G.; Kim, G. Y.; Grätzel, M.; Maier, J. Charge Carrier Chemistry in Methylammonium Lead Iodide. *Solid State Ionics* **2018**, *321*, 69−74.
(47) Merkle, R.; Maier, J. Oxygen Incorporation into Fe-Doped $SrTiO_3$: Mechanistic Interpretation of the Surface Reaction. *Phys. Chem. Chem. Phys.* **2002**, *4* (17), 4140−4148.
(48) Maier, J. Mass Transport in the Presence of Internal Defect Reactions-Concept of Conservative Ensembles: I, Chemical Diffusion in Pure Compounds. *J. Am. Ceram. Soc.* **1993**, *76* (5), 1212−1217.
(49) Maier, J. Mass Transport in the Presence of Internal Defect Reactions-Concept of Conservative Ensembles: III, Trapping Effect of Dopants on Chemical Diffusion. *J. Am. Ceram. Soc.* **1993**, *76* (5), 1223−1227.
(50) Wagner, C. Galvanische Zellen Mit Festen Elektrolyten Mit Gemischter Stromleitung. *Z. Elektrochem., Ber. Bunsenges. Phys. Chem.* **1956**, *60* (1), 4−7.
(51) Hebb, M. H. Electrical Conductivity of Silver Sulfide. *J. Chem. Phys.* **1952**, *20* (1), 185−190.
(52) Yokota, I. On the Theory of Mixed Conduction with Special Reference to Conduction in Silver Sulfide Group Semiconductors. *J. Phys. Soc. Jpn.* **1961**, *16* (11), 2213−2223.
(53) Jamnik, J.; Maier, J. Generalised Equivalent Circuits for Mass and Charge Transport: Chemical Capacitance and Its Implications. *Phys. Chem. Chem. Phys.* **2001**, *3* (9), 1668−1678.
(54) Jamnik, J.; Maier, J. Treatment of the Impedance of Mixed Conductors Equivalent Circuit Model and Explicit Approximate Solutions. *J. Electrochem. Soc.* **1999**, *146* (11), 4183.
(55) Lai, W.; Haile, S. M. Impedance Spectroscopy as a Tool for Chemical and Electrochemical Analysis of Mixed Conductors: A Case Study of Ceria. *J. Am. Ceram. Soc.* **2005**, *88* (11), 2979−2997.
(56) Gregori, G.; Yang, T.-Y.; Senocrate, A.; Grätzel, M.; Maier, J. Ionic Conductivity of Organic-Inorganic Perovskites: Relevance for Long-Time and Low Frequency Behavior. In *Organic-Inorganic Halide Perovskite Photovoltaics*; Park, N.-G., Grätzel, M., Miyasaka, T., Eds.; Springer International Publishing, 2016; pp 107−135.
(57) Maier, J. Mass Transport in the Presence of Internal Defect Reactions-Concept of Conservative Ensembles: II, Evaluation of Electrochemical Transport Measurements. *J. Am. Ceram. Soc.* **1993**, *76* (5), 1218−1222.
(58) Rodewald, S.; Sakai, N.; Yamaji, K.; Yokokawa, H.; Fleig, J.; Maier, J. The Effect of the Oxygen Exchange at Electrodes on the High-Voltage Electrocoloration of Fe-Doped $SrTiO_3$ Single Crystals: A Combined SIMS and Microelectrode Impedance Study. *J. Electroceram.* **2001**, *7* (2), 95−105.
(59) Merkle, R.; Maier, J.; Becker, K. D.; Kreye, M. Chemical Diffusion with Non-Constant D^{δ} and the Appearance of a Parabolic

DOI: 10.1021/jacs.8b13594
J. Am. Chem. Soc. 2019, 141, 8382−8396

Rate Law: Model Study on $SrTiO_3$. *Phys. Chem. Chem. Phys.* **2004**, *6* (13), 3633−3638.
(60) Maier, J. Nanoionics: Ion Transport and Electrochemical Storage in Confined Systems. *Nat. Mater.* **2005**, *4* (11), 805−815.
(61) Gregori, G.; Merkle, R.; Maier, J. Ion Conduction and Redistribution at Grain Boundaries in Oxide Systems. *Prog. Mater. Sci.* **2017**, *89*, 252−305.
(62) Maier, J. Defect Chemistry and Ion Transport in Nanostructured Materials: Part II. Aspects of Nanoionics. *Solid State Ionics* **2003**, *157* (1), 327−334.
(63) Lupetin, P.; Gregori, G.; Maier, J. Mesoscopic Charge Carriers Chemistry in Nanocrystalline $SrTiO_3$. *Angew. Chem., Int. Ed.* **2010**, *49* (52), 10123−10126.
(64) Frost, J. M.; Butler, K. T.; Brivio, F.; Hendon, C. H.; van Schilfgaarde, M.; Walsh, A. Atomistic Origins of High-Performance in Hybrid Halide Perovskite Solar Cells. *Nano Lett.* **2014**, *14* (5), 2584−2590.
(65) Stoumpos, C. C.; Malliakas, C. D.; Kanatzidis, M. G. Semiconducting Tin and Lead Iodide Perovskites with Organic Cations: Phase Transitions, High Mobilities, and Near-Infrared Photoluminescent Properties. *Inorg. Chem.* **2013**, *52* (15), 9019−9038.
(66) Wasylishen, R. E.; Knop, O.; Macdonald, J. B. Cation Rotation in Methylammonium Lead Halides. *Solid State Commun.* **1985**, *56* (7), 581−582.
(67) Knop, O.; Wasylishen, R.; White, M. A.; Cameron, T. S.; van Oort, M. J. M. Alkylammonium Lead Halides. Part 2. $CH_3NH_3PbX_3$ (X = Cl, Br, I) Perovskites: Cubeoctahedral Halide Cages with Isotropic Cation Reorientation. *Can. J. Chem.* **1990**, *68*, 412−422.
(68) Kubicki, D. J.; Prochowicz, D.; Hofstetter, A.; Péchy, P.; Zakeeruddin, S. M.; Grätzel, M.; Emsley, L. Cation Dynamics in Mixed-Cation $(MA)_x(FA)_{1-x}PbI_3$ Hybrid Perovskites from Solid-State NMR. *J. Am. Chem. Soc.* **2017**, *139* (29), 10055−10061.
(69) Senocrate, A.; Moudrakovski, I.; Maier, J. Short-Range Ion Dynamics in Methylammonium Lead Iodide by Multinuclear Solid State NMR and ^{127}I NQR. *Phys. Chem. Chem. Phys.* **2018**, *20* (30), 20043−20055.
(70) Yuan, Y.; Chae, J.; Shao, Y.; Wang, Q.; Xiao, Z.; Centrone, A.; Huang, J. Photovoltaic Switching Mechanism in Lateral Structure Hybrid Perovskite Solar Cells. *Adv. Energy Mater.* **2015**, *5* (15), 1500615.
(71) Leijtens, T.; Hoke, E. T.; Grancini, G.; Slotcavage, D. J.; Eperon, G. E.; Ball, J. M.; De Bastiani, M.; Bowring, A. R.; Martino, N.; Wojciechowski, K.; et al. Mapping Electric Field-Induced Switchable Poling and Structural Degradation in Hybrid Lead Halide Perovskite Thin Films. *Adv. Energy Mater.* **2015**, *5* (20), 1500962.
(72) Senocrate, A.; Moudrakovski, I.; Kim, G. Y.; Yang, T.-Y.; Gregori, G.; Grätzel, M.; Maier, J. The Nature of Ion Conduction in Methylammonium Lead Iodide: A Multimethod Approach. *Angew. Chem., Int. Ed.* **2017**, *56* (27), 7755−7759.
(73) Mizusaki, J.; Arai, K.; Fueki, K. Ionic Conduction of the Perovskite-Type Halides. *Solid State Ionics* **1983**, *11* (3), 203−211.
(74) Yamada, K.; Isobe, K.; Okuda, T.; Furukawa, Y. Successive Phase Transitions and High Ionic Conductivity of Trichlorogermanate (II) Salts as Studied by ^{35}Cl NQR and Powder X-Ray Diffraction. *Z. Naturforsch. A* **1994**, *49* (1−2), 258−266.
(75) Yamada, K. Chloride Ion Conductor $CH_3NH_3GeCl_3$ Studied by Rietveld Analysis of X-Ray Diffraction and ^{35}Cl NMR. *Solid State Ionics* **1995**, *79*, 152−157.
(76) Yamada, K.; Kuranaga, Y.; Ueda, K.; Goto, S.; Okuda, T.; Furukawa, Y. Phase Transition and Electric Conductivity of $ASnCl_3$ (A = Cs and CH_3NH_3). *Bull. Chem. Soc. Jpn.* **1998**, *71* (1), 127−134.
(77) Walsh, A.; Scanlon, D. O.; Chen, S.; Gong, X. G.; Wei, S.-H. Self-Regulation Mechanism for Charged Point Defects in Hybrid Halide Perovskites. *Angew. Chem., Int. Ed.* **2015**, *54* (6), 1791−1794.
(78) Yin, W.-J.; Shi, T.; Yan, Y. Unusual Defect Physics in $CH_3NH_3PbI_3$ Perovskite Solar Cell Absorber. *Appl. Phys. Lett.* **2014**, *104* (6), 063903.
(79) Kim, J.; Lee, S.-H.; Lee, J. H.; Hong, K.-H. The Role of Intrinsic Defects in Methylammonium Lead Iodide Perovskite. *J. Phys. Chem. Lett.* **2014**, *5* (8), 1312−1317.
(80) Eames, C.; Frost, J. M.; Barnes, P. R. F.; O'Regan, B. C.; Walsh, A.; Islam, M. S. Ionic Transport in Hybrid Lead Iodide Perovskite Solar Cells. *Nat. Commun.* **2015**, *6* (1), 7497.
(81) Haruyama, J.; Sodeyama, K.; Han, L.; Tateyama, Y. First-Principles Study of Ion Diffusion in Perovskite Solar Cell Sensitizers. *J. Am. Chem. Soc.* **2015**, *137* (32), 10048−10051.
(82) Azpiroz, J. M.; Mosconi, E.; Bisquert, J.; De Angelis, F. Defect Migration in Methylammonium Lead Iodide and Its Role in Perovskite Solar Cell Operation. *Energy Environ. Sci.* **2015**, *8* (7), 2118−2127.
(83) Ivanov, I. L.; Steparuk, A. S.; Bolyachkina, M. S.; Tsvetkov, D. S.; Safronov, A. P.; Zuev, A. Y. Thermodynamics of Formation of Hybrid Perovskite-Type Methylammonium Lead Halides. *J. Chem. Thermodyn.* **2018**, *116*, 253−258.
(84) Barboni, D.; De Souza, R. A. The Thermodynamics and Kinetics of Iodine Vacancies in the Hybrid Perovskite Methylammonium Lead Iodide. *Energy Environ. Sci.* **2018**, *11* (11), 3266−3274.
(85) Quilitz, M.; Maier, J. Defect Chemistry and Oxygen Transport in $Bi_2Sr_2CaCu_2O_{8+\delta}$ derived from Conductivity, Polarization, and Hall Effect Measurements. *J. Supercond.* **1996**, *9* (1), 121−127.
(86) Besleaga, C.; Abramiuc, L. E.; Stancu, V.; Tomulescu, A. G.; Sima, M.; Trinca, L.; Plugaru, N.; Pintilie, L.; Nemnes, G. A.; Iliescu, M.; et al. Iodine Migration and Degradation of Perovskite Solar Cells Enhanced by Metallic Electrodes. *J. Phys. Chem. Lett.* **2016**, *7* (24), 5168−5175.
(87) Li, J.; Dong, Q.; Li, N.; Wang, L. Direct Evidence of Ion Diffusion for the Silver-Electrode-Induced Thermal Degradation of Inverted Perovskite Solar Cells. *Adv. Energy Mater.* **2017**, *7* (14), 1602922.
(88) Li, C.; Guerrero, A.; Zhong, Y.; Gräser, A.; Luna, C. A. M.; Köhler, J.; Bisquert, J.; Hildner, R.; Huettner, S. Real-Time Observation of Iodide Ion Migration in Methylammonium Lead Halide Perovskites. *Small* **2017**, *13* (42), 1701711.
(89) Domanski, K.; Roose, B.; Matsui, T.; Saliba, M.; Turren-Cruz, S.-H.; Correa-Baena, J.-P.; Carmona, C. R.; Richardson, G.; Foster, J. M.; De Angelis, F.; et al. Migration of Cations Induces Reversible Performance Losses over Day/Night Cycling in Perovskite Solar Cells. *Energy Environ. Sci.* **2017**, *10* (2), 604−613.
(90) Yuan, Y.; Wang, Q.; Shao, Y.; Lu, H.; Li, T.; Gruverman, A.; Huang, J. Electric-Field-Driven Reversible Conversion Between Methylammonium Lead Triiodide Perovskites and Lead Iodide at Elevated Temperatures. *Adv. Energy Mater.* **2016**, *6* (2), 1501803.
(91) Jacobs, D. A.; Wu, Y.; Shen, H.; Barugkin, C.; Beck, F. J.; White, T. P.; Weber, K.; Catchpole, K. R.; Snaith, H. J.; Hodes, G.; et al. Hysteresis Phenomena in Perovskite Solar Cells: The Many and Varied Effects of Ionic Accumulation. *Phys. Chem. Chem. Phys.* **2017**, *19* (4), 3094−3103.
(92) Contreras, L.; Idígoras, J. A.; Todinova, A.; Salado, M.; Kazim, S.; Ahmad, S.; Anta, J. Specific Cation Interactions as the Cause of Slow Dynamics and Hysteresis in Dye and Perovskite Solar Cells: A Small-Perturbation Study. *Phys. Chem. Chem. Phys.* **2016**, *18*, 31033−31042.
(93) Xia, H.-R.; Sun, W.-T.; Peng, L.-M. Hydrothermal Synthesis of Organometal Halide Perovskites for Li-Ion Batteries. *Chem. Commun.* **2015**, *51* (72), 13787−13790.
(94) Li, Z.; Xiao, C.; Yang, Y.; Harvey, S. P.; Kim, D. H.; Christians, J. A.; Yang, M.; Schulz, P.; Nanayakkara, S. U.; Jiang, C.-S.; et al. Extrinsic Ion Migration in Perovskite Solar Cells. *Energy Environ. Sci.* **2017**, *10* (5), 1234−1242.
(95) Domanski, K.; Correa-Baena, J. P.; Mine, N.; Nazeeruddin, M. K.; Abate, A.; Saliba, M.; Tress, W.; Hagfeldt, A.; Grätzel, M. Not All That Glitters Is Gold: Metal-Migration-Induced Degradation in Perovskite Solar Cells. *ACS Nano* **2016**, *10* (6), 6306−6314.
(96) Pellet, N.; Teuscher, J.; Maier, J.; Grätzel, M. Transforming Hybrid Organic Inorganic Perovskites by Rapid Halide Exchange. *Chem. Mater.* **2015**, *27* (6), 2181−2188.

DOI: 10.1021/jacs.8b13594
J. Am. Chem. Soc. 2019, 141, 8382−8396

(97) Nedelcu, G.; Protesescu, L.; Yakunin, S.; Bodnarchuk, M. I.; Grotevent, M. J.; Kovalenko, M. V. Fast Anion-Exchange in Highly Luminescent Nanocrystals of Cesium Lead Halide Perovskites ($CsPbX_3$, X = Cl, Br, I). *Nano Lett.* **2015**, *15* (8), 5635−5640.
(98) Akkerman, Q. A.; D'Innocenzo, V.; Accornero, S.; Scarpellini, A.; Petrozza, A.; Prato, M.; Manna, L. Tuning the Optical Properties of Cesium Lead Halide Perovskite Nanocrystals by Anion Exchange Reactions. *J. Am. Chem. Soc.* **2015**, *137* (32), 10276−10281.
(99) Senocrate, A.; Moudrakovski, I.; Acartürk, T.; Merkle, R.; Kim, G. Y.; Starke, U.; Grätzel, M.; Maier, J. Slow $CH_3NH_3^+$ Diffusion in $CH_3NH_3PbI_3$ under Light Measured by Solid-State NMR and Tracer Diffusion. *J. Phys. Chem. C* **2018**, *122* (38), 21803−21806.
(100) Eperon, G. E.; Beck, C. E.; Snaith, H. J. Cation Exchange for Thin Film Lead Iodide Perovskite Interconversion. *Mater. Horiz.* **2016**, *3* (1), 63−71.
(101) Xie, Y.; Yu, B.; Ma, C.; Xu, X.; Cheng, Y.; Yuan, S.; Wang, Z.-K.; Chandran, H. T.; Lee, C.; Liao, L.-S.; et al. Direct Observation of Cation-Exchange in Liquid-to-Solid Phase Transformation in $FA_{1-x}MA_xPbI_3$ Based Perovskite Solar Cells. *J. Mater. Chem. A* **2018**, *6*, 9081−9088.
(102) Kim, G. Y.; Senocrate, A.; Moia, D.; Maier, J. Ionically generated built-in equilibrium space charge zones−a paradigm change for lead halide perovskite interfaces, to be submitted for publication.
(103) Xing, J.; Wang, Q.; Dong, Q.; Yuan, Y.; Fang, Y.; Huang, J. Ultrafast Ion Migration in Hybrid Perovskite Polycrystalline Thin Films under Light and Suppression in Single Crystals. *Phys. Chem. Chem. Phys.* **2016**, *18* (44), 30484−30490.
(104) Zhao, Y.-C.; Zhou, W.-K.; Zhou, X.; Liu, K.; Yu, D.; Zhao, Q. Quantification of Light-Enhanced Ionic Transport in Lead Iodide Perovskite Thin Films and Its Solar Cell Applications. *Light: Sci. Appl.* **2016**, *6* (5), No. e16243.
(105) Song, K. S.; Williams, R. T. *Self-Trapped Excitons*; Springer Series in Solid-State Sciences; Springer: Berlin/Heidelberg, 1993; Vol. *105*.
(106) Castner, T. G.; Känzig, W. The Electronic Structure of V-Centers. *J. Phys. Chem. Solids* **1957**, *3* (3−4), 178−195.
(107) Wilson, D. J.; Sokol, A. A.; French, S. A.; Catlow, C. R. A. Defect Structures in the Silver Halides. *Phys. Rev. B: Condens. Matter Mater. Phys.* **2008**, *77* (6), 064115.
(108) Popov, A. I.; Kotomin, E. A.; Maier, J. Analysis of Self-Trapped Hole Mobility in Alkali Halides and Metal Halides. *Solid State Ionics* **2017**, *302*, 3−6.
(109) Hoke, E. T.; Slotcavage, D. J.; Dohner, E. R.; Bowring, A. R.; Karunadasa, H. I.; McGehee, M. D. Reversible Photo-Induced Trap Formation in Mixed-Halide Hybrid Perovskites for Photovoltaics. *Chem. Sci.* **2015**, *6* (1), 613−617.
(110) Zhou, Y.; You, L.; Wang, S.; Ku, Z.; Fan, H.; Schmidt, D.; Rusydi, A.; Chang, L.; Wang, L.; Ren, P.; et al. Giant Photostriction in Organic-inorganic Lead Halide Perovskites. *Nat. Commun.* **2016**, *7* (1), 11193.

DOI: 10.1021/jacs.8b13594
J. Am. Chem. Soc. 2019, 141, 8382−8396